ACS APPLIED NANO MATERIALS

www.acsanm.org Article

Bandgap-Engineered $CsPbBr_{3x}I_{3-3x}$ Alloy Nanowires for Broadly Tunable Nanoscale Lasers

Jie Fan, Pengfei Guo,* Qihang Lv, Xia Shen,* Xiaohang Song, You Meng, Zitong Xu, Jishen Wang, Tingkai Xu, Xuyang Li, Liantuan Xiao, and Johnny C. Ho

Cite This: *ACS Appl. Nano Mater.* 2023, 6, 17881−17889 Read Online

ACCESS | Metrics & More | Article Recommendations | Supporting Information

ABSTRACT: Halide perovskite nanowires (NWs) have excellent photoelectric properties, such as high quantum efficiency and carrier mobility, and are ideal candidates for next-generation optoelectronic devices and circuits. In particular, all-inorganic perovskite materials have a soft and dynamic crystal lattice, tunable bandgaps, better thermal stability, etc., which make them ideal candidates for wavelength-tunable emitters and full-color displays. Here, we reported an anion exchange method to synthesize bandgap-modulated $CsPbBr_{3x}I_{3-3x}$ alloy NWs on SiO_2/Si substrate. These NWs have smooth end surfaces and exhibit NW lasing with a threshold of 18.09 μJ cm^{-2} and a high-quality factor of 633−1075. Moreover, under a 355 nm pulse laser illumination, room-temperature wavelength continuous tunable lasing ranging from 538 to 699 nm is realized using these bandgap-tunable perovskite NWs. The growth strategies of these bandgap-graded structures may offer an interesting system for enriching the synthesis methods of alloy perovskites and exploring applications in multifunctional nanophotonic and optoelectronic devices.

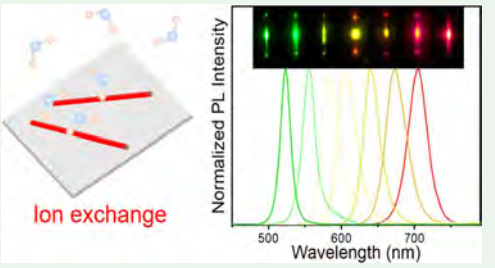

KEYWORDS: *perovskite nanowires, anion exchange process, one-step chemical vapor deposition, bandgap modulation, tunable laser*

1. INTRODUCTION

Bandgap modulation in semiconductor materials plays an extremely important role in developing nanoscience and technology.[1−7] Semiconductor materials with different bandgaps will exert a unique role in the field of optoelectronic devices such as photodetectors,[8−11] lasers,[4,6,12−14] light-emitting diodes,[15,16] waveguides,[17,18] and solar cells.[19−23] However, the utilized bandgaps of natural semiconductors are very limited for the continuously developed technology, and the traditional semiconductor materials are difficult to meet the needs of integrated photoelectronic devices and circuits.[24] Therefore, integrating different components to construct semiconductor alloys with flexible bandgaps has become increasingly challenging in recent years.[7,25−27] Presently, adjusting the composition by ion exchange has been proven to be an effective method for fabricating semiconductor alloys.[28−33] In general, the ion exchange reaction is driven by the ion concentration difference between the reactant and the reaction environment, and the alloy material is formed by the diffusion of high-concentration ions in the reaction environment in the low-concentration reactant.[34] Due to the advantages of simple operation and fine adjustment of physical properties, the ion exchange method has played a crucial role in the development of semiconductor materials.[31,35,36] It has been a common method to synthesize homogeneous alloys,[8,11,14,37] core−shell heterostructures[38,39] and nanowire (NW) heterostructures.[40−42] Perovskite has a soft and dynamic crystal lattice because of its fragile ionic bonds and high concentration of vacancies.[40,43,44] Moreover, perovskite materials have low defect formation energy, which allows ion diffusion and migration in the lattice and acts as an ideal material for ion exchange reactions.[45] In addition, halide perovskites have the advantages of long carrier diffusion length,[46,−53] high PL quantum yield,[54−56] and high defect tolerance,[57−59] which make them ideal candidates for next-generation optoelectronic circuits.

Therefore, it is an effective way to tune the bandgap by adjusting the composition of halide perovskites through ion exchange processes.[6,58,60] For example, in 2016, Fu et al. reported the growth of $CsPbCl_3$, $CsPbBr_3$, and $CsPbCl_{3x}Br_{3-3x}$ NWs by a solution-phase synthesis method.[61] The $CsPbBr_{3x}I_{3-3x}$ NWs were grown by an ion exchange reaction using $C_4H_9NH_3I$ as an anion source.[61] Room-temperature lasers with low thresholds and high quality are realized based on these NWs. In 2017, Yang et al. reported the growth of $CsPbX_3$ (X = Cl, Br, I) semiconductor NW heterojunctions by anion exchange process, which claimed to realize a single perovskite heterojunction with red-green-blue emissions along the wire.[40] In 2019, Jin et al. reported the dynamic diffusion process between $CsPbCl_3$ microplates and $CsPbBr_3$ NWs stacked to

Received: July 10, 2023
Accepted: September 15, 2023
Published: September 27, 2023

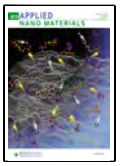

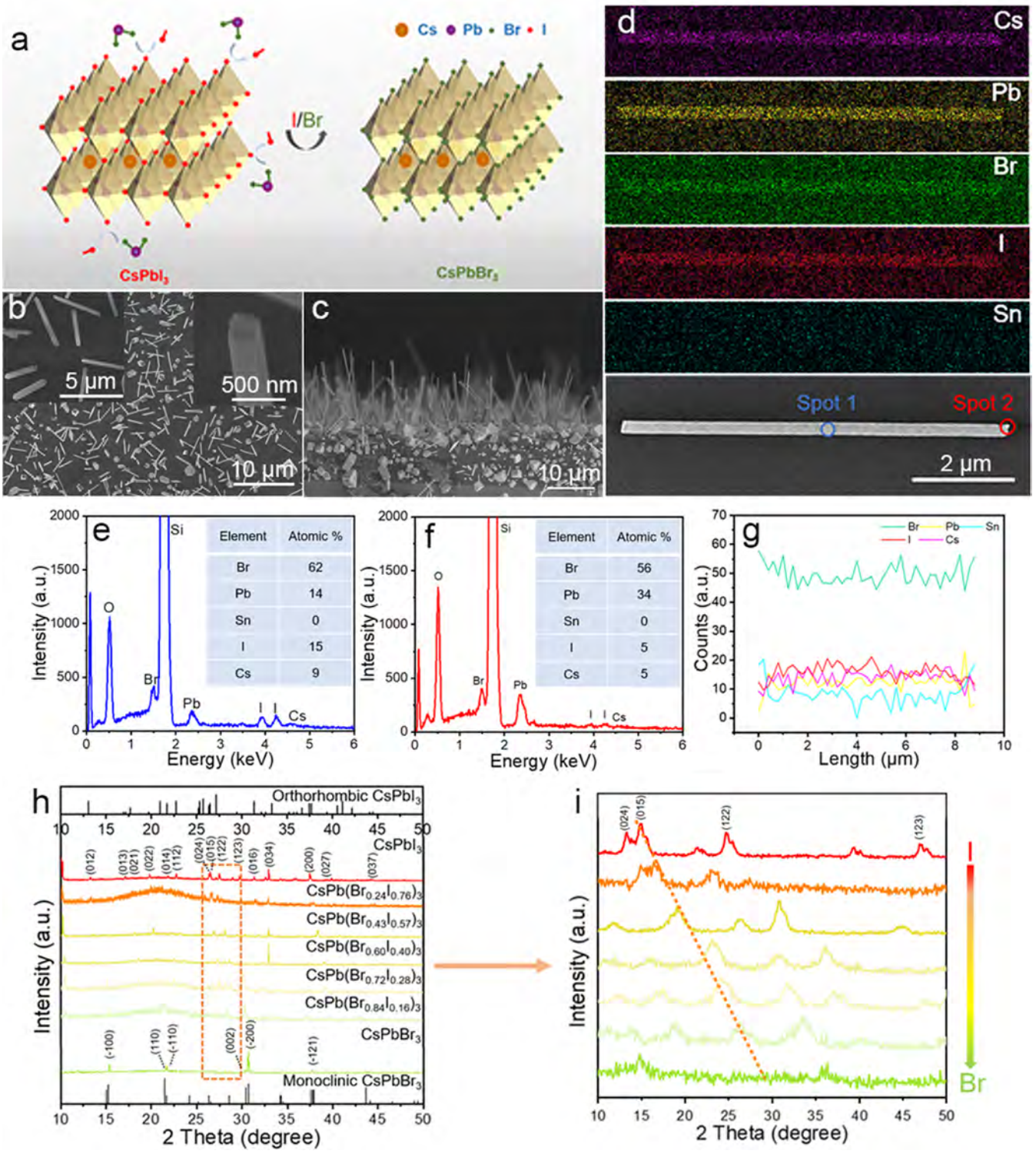

Figure 1. (a) Atomic structure scheme of $CsPbBr_3$ and $CsPbI_3$. (b, c) Low-resolution top-view SEM image and high-resolution SEM image (inset) of the $CsPbBr_{3x}I_{3-3x}$ alloy perovskite NWs with a rectangular cross section grown on a substrate. (d) SEM image and EDX element mapping of a typical alloy NW show the uniform spatial distribution of Cs, Pb, Br, and I. (e, f) EDX element scanning profiles of a single alloy NW at spots 1 and 2, respectively. (g) Line scanning EDX profile of an NW along the axial direction. (h) XRD patterns of $CsPbBr_{3x}I_{3-3x}$ nanostructures with different compositions ranging from 10 to 50°. The corresponding standard cards of the orthorhombic phase $CsPbI_3$ (no.18−0376) and monoclinic phase $CsPbBr_3$ (no.18−0364) are also shown in (h), respectively. (i) Enlarged XRD patterns ranging from 26 to 30°.

form $CsPbCl_3$−$CsPbBr_3$ heterostructures by solid-phase anion exchange process.[29] These findings further demonstrated that the anion exchange method played an important role in bandgap modulation.

Here, we report the growth of high-quality $CsPbBr_3$, $CsPbI_3$, and $CsPbBr_{3x}I_{3-3x}$ (x = 0−1) alloy NWs by a simple magnetic-pulling source-moving chemical vapor deposition (CVD) method. Different compositions of $CsPbBr_{3x}I_{3-3x}$ alloy NWs

https://doi.org/10.1021/acsanm.3c03173
ACS Appl. Nano Mater. 2023, 6, 17881−17889

are synthesized using a controllable ion exchange process by changing the temperature and reaction time. The as-grown NWs have high-quality crystalline with excellent and smooth rectangular sections. Under a 375 nm laser illumination, the emission colors of these perovskite NWs can be tuned from green (523 nm) to red (706 nm) continuously. Moreover, these NWs can be used as a Fabry−Perot (F−P) resonator to achieve tunable nanoscale lasers with wavelengths ranging from 538 to 699 nm, and the laser threshold and Q factor can be reached to 18.09 μJ cm^{-2} and 1075, respectively. These prepared $CsPbBr_3$, $CsPbI_3$, and $CsPbBr_{3x}I_{3-3x}$ alloy NWs may have potential applications for full-color displays and solid-state lighting in the future.

2. EXPERIMENTAL SECTION

2.1. Synthesis of Pure $CsPbBr_3$ and $CsPbI_3$ NWs. Pure $CsPbBr_3$ and $CsPbI_3$ NWs were grown vertically on the SiO_2/Si substrates (4 mm × 10 mm) via a CVD method. A 2 in. quartz tube (45 mm in diameter, 180 cm in length) was sited inside the tube furnace (OTF-1200X). First, 0.1 mg/mL of Sn solution was dropped on the substrate and used as a catalyst. The quartz boat, containing PbI_2/CsI or CsBr/$PbBr_2$ mixed powders (molar ratio 2:1), was placed in the heating area of the quartz tube (Figure S1a, Supporting Information). The substrate was positioned downstream of the quartz tube. Before heating, N_2 gas was introduced into the system at a flow rate of 60 sccm for 30 min to purge the air and moisture from the tube. The carrier gas (40 sccm H_2 and 50 sccm N_2) was introduced into the system, and the pressure was kept at 5.82 Torr while growing $CsPbI_3$ NWs. Also, the pressure (5.80 Torr) has little difference when growing $CsPbBr_3$ NWs. The heating temperature (zone A) of the quartz tube was increased to 420 °C at a rate of 25 °C min^{-1} (390 °C when growing $CsPbBr_3$ NWs), and the deposition temperature of the quartz tube was increased to 290 °C at a rate of 25 °C min^{-1} at zone B. After the growth of 60 min, the furnace was cooled down to natural.

2.2. Synthesis of $CsPbBr_{3x}I_{3-3x}$ Alloy NWs. The magnetic-pulling source-moving CVD method was used to synthesize $CsPbBr_{3x}I_{3-3x}$ alloy NWs. Two boats with CsI/PbI_2 mixed and CsBr/$PbBr_2$ mixed powders were located in zone A and connected with a quartz rod. First, the boat with CsI/PbI_2 powder was placed in zone A, and the single-component $CsPbI_3$ NWs were synthesized by the CVD method. Then, the second boat with CsBr/$PbBr_2$ powder was moved to zone A using a step motor, while the first boat was moved to zone B (Figure S1b, Supporting Information). The pressure and temperature were set at 5.80 Torr and 390 °C, respectively. Under high temperatures, $CsPbBr_{3x}I_{3-3x}$ alloy NWs were obtained by controlling the growth time, and the ratio of Br can be controlled through the second growth process.

2.3. Characterization. The morphology of these alloy NWs was investigated via scanning electron microscopy (SEM, Hitachi S-4800) and energy-dispersive X-ray spectroscopy (EDX). The crystallinity of these alloy NWs was investigated by X-ray diffraction (XRD). The optical images and PL spectra of NWs were tested by a self-made confocal optical system. The laser beam (375 nm, spot size, 1.5 μm) was focused to a spot size of ∼0.8 μm by a microscope lens (Nikon, ×100) and locally excited at the NWs. The PL spectra were recorded by an optical spectrometer (Maya Pro2000), and real-color images were recorded by a CCD camera. The stimulated emission characteristics were studied using 355 nm pulse laser illumination, which was focused to 100 μm.

3. RESULTS AND DISCUSSION

Figure 1a shows the atomic structure scheme of perovskite. Perovskite has an octahedral structure with the chemical formula ABX_3, the inorganic cation Cs^+ located at the corner centers, the cation Pb^{2+} located at the body centers, and the halide anion I^- located at the face centers. A gas-phase anion exchange method was used to form alloy NWs through the replacement of Br^- for I^-. Figure 1b and the inset image show the SEM images of the $CsPbBr_{3x}I_{3-3x}$ alloy NWs. The length of NWs is about 10−25 μm, and the diameter is ∼300−500 nm. Both ends of a typical $CsPbBr_{3x}I_{3-3x}$ (x = 0−1) NW show a clear and smooth rectangular face with a catalyst at the tip of the NW (Figures 1b and S2, Supporting Information). Side-view SEM (Figure 1c) shows that most of the NWs are grown vertically to the substrate or slightly inclined to the substrate. This bottle-up growth process indicates that the NWs are prepared through the vapor−liquid−solid (VLS) growth mechanism. In addition, the pure $CsPbI_3$ NWs exhibit similar morphology with the $CsPbBr_{3x}I_{3-3x}$ alloy perovskite NWs as shown in Figure S3 (Supporting Information). To further confirm the role of Sn and growth mechanism, a mask technique was used to achieve patterned growth of $CsPbI_3$ NWs (Figure S4, Supporting Information). The SiO_2/Si substrate with/without dropped Sn catalysts is shown in Figure S4b (Supporting Information) using a mask, which shows a clear demarcation line between the two regions. After that, this substrate was used to grow $CsPbI_3$ NWs, and the NWs are only grown in the region with Sn catalysts, and almost no deposition on the Sn-free region (see Figure S4c,d, Supporting Information). Under a 405 nm laser illumination, these as-grown $CsPbI_3$ NWs exhibit red color emission with a wavelength of 706 nm (see Figure S4e,f, Supporting Information), respectively. The experimental results are consistent with the mechanism of VLS growth. The morphology and element distribution of a typical $CsPbBr_{3x}I_{3-3x}$ alloy NWs are observed by SEM and EDX. As shown in Figure 1d, Cs, Pb, Br, and I show uniform spatial distribution along the wire. Sn is scattered in various positions on the substrate. The EDX profiles at the body and tip of the NW are shown in Figure 1e,f, which indicates that the as-grown wires are $CsPbBr_{2.4}I_{0.6}$ alloy NW with a catalyst at the wire tip. The EDX element line scanning profile of the same alloy NW along the axial direction is shown in Figure 1g, which shows agreement with the two-dimensional (2D) EDX elemental mapping results. Notably, Pb exhibits a sudden increase at the tip of the NW, which indicates that the nanosphere catalyst at the tip of the NW is composed of Pb, further indicating a VLS growth mechanism of the NWs. The high-resolution SEM image, 2D elemental mapping, and line scanning elemental profiles of a typical NW further confirmed that the NWs are homogeneous alloy structures rather than core−shell structures (Figure S5, Supporting Information).

Figure 1h shows the XRD patterns of these perovskite NWs ranging from 10 to 50°, the sharp diffraction peaks confirming that these bandgap-tunable $CsPbBr_{3x}I_{3-3x}$ alloy nanostructures are excellent crystalline. After the anion exchange, a sharp diffraction peak at 30.68° appeared, corresponding to the (−200) plane of monoclinic phase $CsPbBr_3$. The enlarged XRD patterns from 26 to 30°, as indicated in Figure 1h, are shown in Figure 1i, further exhibiting the peak shift of the diffraction peaks. These diffraction peaks corresponding to the (015) plane are slightly shifted toward the high-angle region compared with pure $CsPbI_3$ NWs, as the lattice shrunk with the increased amount of Br^-, which has a smaller ion radius than that of I^-, indicating that these $CsPbBr_{3x}I_{3-3x}$ alloys could be fabricated using this simple anion exchange method. In 2017, Pan's group reported a similar alloy triangular rod structure and performed TEM analysis of $CsPbBr_3$ NWs with a lattice spacing of 0.29 nm.[6] Subsequently, they demonstrated some alloy nanostructures with stimulated emission wavelengths in the range of 428−668 nm. Similar alloy nanostructures were also reported by Jin's

https://doi.org/10.1021/acsanm.3c03173
ACS Appl. Nano Mater. 2023, 6, 17881−17889

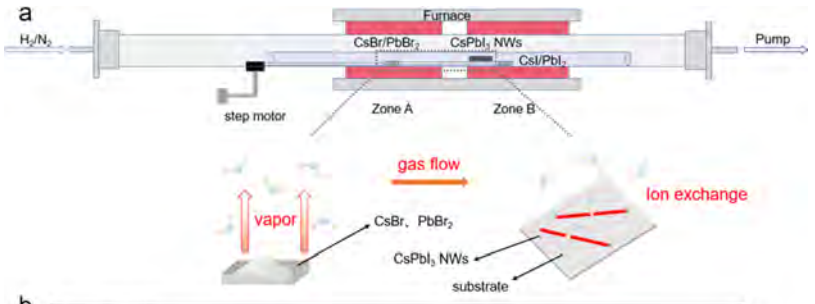

b

T(°C) \ t(min) x(Br)	0	10	20	30	40	50	60	70	80	90	100	110
390	0	0.09	0.31	0.36	0.43	0.55	0.72	0.78	0.84	0.87	0.94	1
420	0	0.68	0.87	1								
440	0	1										

Figure 2. (a) Schematic diagram of the experimental setup and growth process. (b) Relationship between x (composition ratio of Br in $CsPbBr_{3x}I_{3-3x}$ alloy NWs) and the growth temperature and growth time of the anion exchange process.

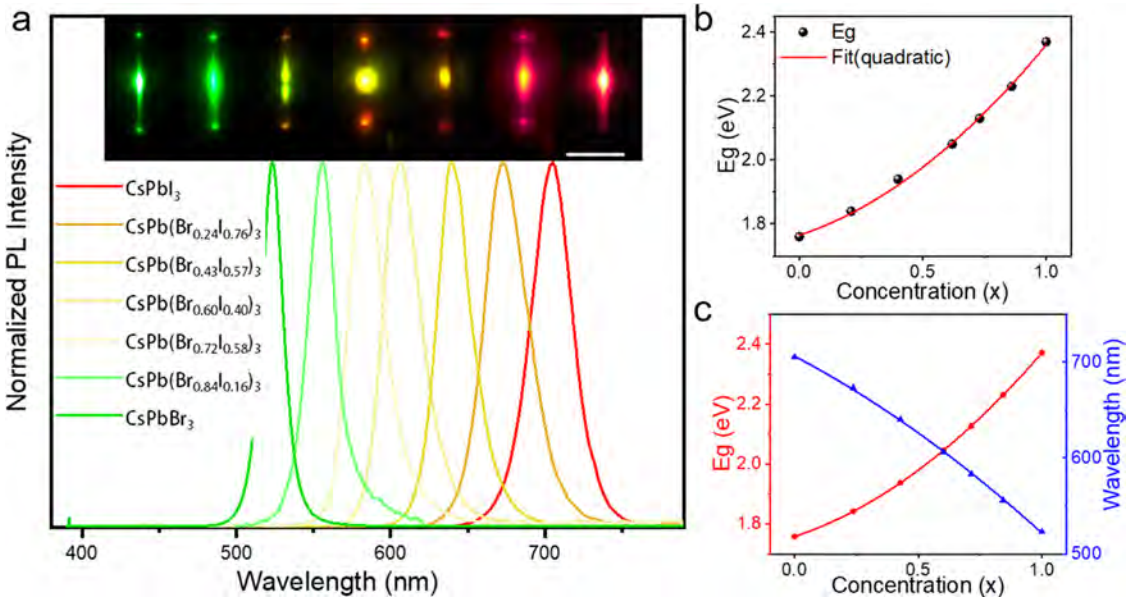

Figure 3. (a) Real-color images and corresponding PL spectra of $CsPbBr_{3x}I_{3-3x}$ alloy NWs with various compositions. The scale bar is 10 μm. (b) Relationship between the bandgap and the composition ratio of Br in alloy NWs obtained by EDX profiles. The black square is the experimental data, and the red solid line is the fitting line. (c) Relationship between the emission wavelengths and bandgaps of $CsPbBr_{3x}I_{3-3x}$ NWs. Red circles represent the bandgaps of $CsPbBr_{3x}I_{3-3x}$ NWs, and blue triangles represent the wavelength of the emission peaks.

group in 2016,[61] in which the excited emission wavelengths were ranging from 400 to 750 nm.

The schematic diagram of the CVD setup and growth diagram of the alloy perovskite NWs are shown in Figure 2a. First, the vacuum pump is used to extract the air from the tube and prevent sample oxidation to create ideal growth conditions for growing NWs. Pure $CsPbI_3$ NWs are synthesized by the CVD method under a high temperature as shown in the Experimental Section. CsBr and $PbBr_2$ powders are placed in the center of the heating zone A, which are used as the anion exchange sources. Second, the vapor sources are flowed to the deposition zone B by the carrier gas and perform an anion exchange reaction with pure $CsPbI_3$ inside the tube. Lastly, the anion sources are diffused in $CsPbI_3$ NWs, forming the $CsPbBr_{3x}I_{3-3x}$ homogeneous alloy NWs. Compared with other synthesis methods of perovskite alloy structures, CVD is attractive for growing diverse NWs with easy setup, low-cost, mild operation, and high-yield advantages.

Compared to other reports on the synthesis of perovskite NWs by vapor phase deposition,[46,47,62] our results demonstrate a flexible bandgap modulation method based on the alloyed perovskite materials.[48] In addition, a one-step anion exchange process is reported in our work, which is better than the two-step synthesis of alloy NWs.[61] It is worth noting that our method could avoid the interference of the air environment and the generation of nonperovskite structures, which may affect the optical properties and crystallinity of the perovskite NWs. The relationship between anion exchange time and the composition ratio of Br (x) is shown in Figure 2b. As can be seen, it takes 110 min to complete the replacement from $CsPbI_3$ to $CsPbBr_3$ at 390 °C. At the same time, the entire ion exchange reaction is much faster at 420 °C (within 30 min) and 440 °C (within 10 min), respectively. Therefore, this one-step growth strategy with tunable heating temperature and moving sources is an effective

https://doi.org/10.1021/acsanm.3c03173
ACS Appl. Nano Mater. 2023, 6, 17881−17889

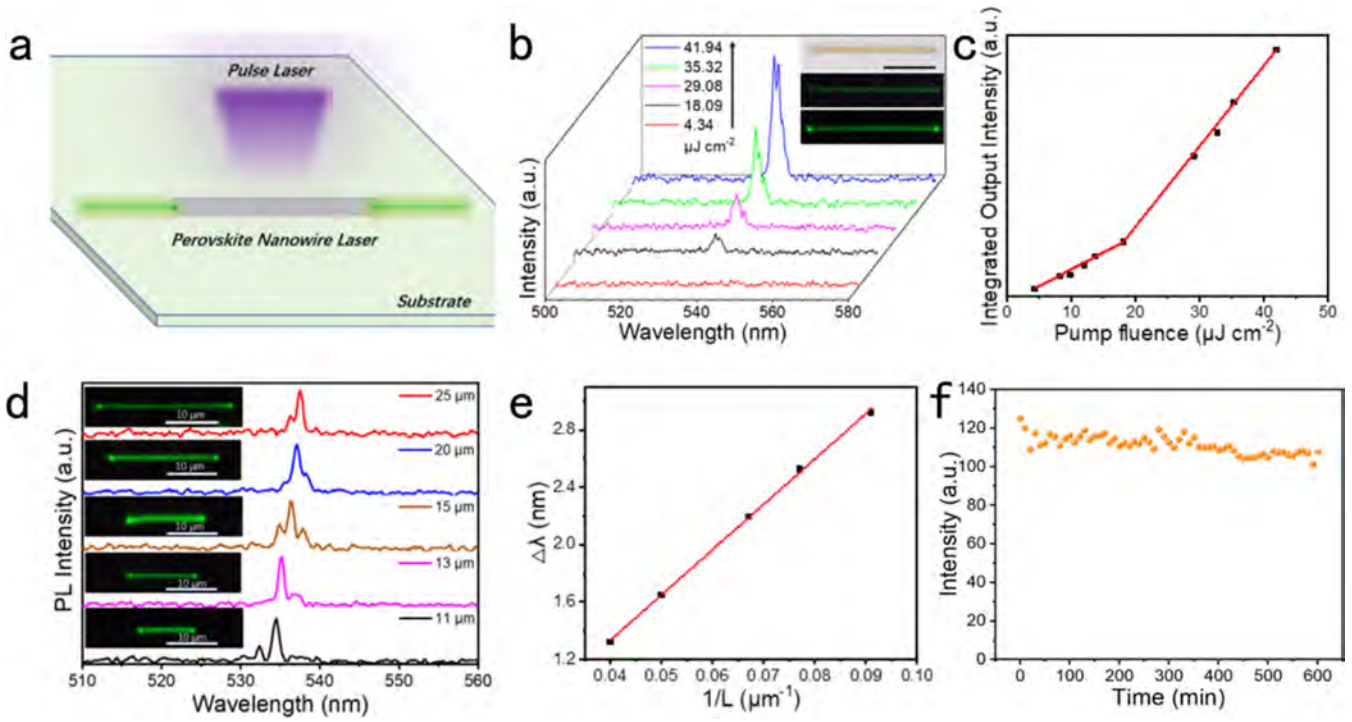

Figure 4. (a) Schematic diagram of NW lasers pumped by a 355 nm pump laser. (b) Room-temperature PL spectra of $CsPbBr_3$ NW under a 355 nm pulse laser excitation. Insets: Bright and dark optical images of $CsPbBr_3$ NWs from spontaneous emission to stimulated emission under low and high pumping power density. The scale bar is 10 μm. (c) Nonlinear response of output intensity with the increasing pump flux. (d) Size-dependent laser emission of $CsPbBr_3$ NWs with wires length from 11 to 25 μm. Insets are dark-field real-color images of NWs with different sizes. The scale bar is 10 μm. (e) Relationship between wire length and mode spacing in (d). The black square is the mode spacing calculated by the experimental data, and the red line is the fitted line of the experimental data. (f) Emission stability of the $CsPbBr_3$ NWs.

way to control the ion exchange reactions, which is considered useful for synthesizing high-quality perovskite alloys.

Room-temperature PL properties of the samples were studied by confocal optical microscopy, as shown in Figure S6 (Supporting Information). Figure 3a shows the PL spectra and corresponding dark-field emission images of these perovskite alloy NWs under 375 nm laser excitation. With the increase of reaction time, the value x is increased from 0 to 1, and the compositions of NWs are changed from $CsPbI_3$ to $CsPbBr_{3x}I_{3-3x}$ and then $CsPbBr_3$ continuously. Insets in Figure 3a exhibit the dark-field real-color image of these composition tunable perovskite structures that change from red, orange, and yellow to green, showing the continuous variation of the emission peak because of different compositions. The bright emission spots at both ends of the wires under laser illumination indicate that these wires have excellent waveguiding, which may have potential applications in high-quality F−P optical resonators. Meanwhile, the emission peaks are continuously tuned from 523 to 706 nm with full width at half-maximum (fwhm) of about 20−30 nm, indicating intrinsic band-to-band emissions of the perovskite NWs. Notably, the fwhm of these PL spectra are smaller than those of nanocrystals synthesized by solution-phase method, which confirms that these synthesized wires may have well-uniform and high crystallization.[63] Figure 3b shows the relationship between the Br composition x and the bandgap values of $CsPbBr_{3x}I_{3-3x}$ obtained by EDX profiles (Figure S7, Supporting Information). The bandgap values of $CsPbBr_{3x}I_{3-3x}$ are also obtained by PL spectra in Figure 3c. According to the relationship between the bandgap E_g and x,[60]

$$E_g = 2.371x + 1.758(1 - x) - bx(1 - x)$$

where x represents the proportion of elemental components of Br, and 2.371 and 1.758 represent the bandgaps of $CsPbBr_3$ and $CsPbI_3$ respectively, and finally the bandgap of $CsPbBr_{3x}I_{3-3x}$ is obtained. According to the calculation result, the curve obtained by the EDX profiles is basically consistent with the fitting curve of the calculated results. Figure 3c plots the relationship between the emission wavelengths and bandgaps of $CsPbBr_{3x}I_{3-3x}$ NWs. The solid line shows the best fit of composition-dependent bandgaps using the virtual crystal approximation with a bowing parameter b = 0.34 eV. All of these results indicate that these perovskite alloy NWs have excellent luminescence properties without obvious defect emissions.

More importantly, tunable nanoscale lasers are reported as good applications based on these alloy perovskite NWs. A 355 nm pulse laser is focused and excited at the NWs, as schematically shown in Figure 4a. Figure 4b shows the pumping-power-dependent PL spectra of $CsPbBr_3$ NWs. When the pump power is higher than the threshold of 18.09 μJ cm^{-2}, a sharp emission peak centered at 537.36 nm appears. The intensity of the emission peak increases rapidly with the increase of pumping power density, which represents a lasing action of NWs in Figure 4c. The real-color images below and above the threshold and the optical photograph of a single $CsPbBr_3$ NW are shown in the inset of Figure 4d. As can be seen, under high pumping power density, bright output emissions occur at both ends of NWs, confirming the transition from spontaneous emission to stimulated emission of NWs.[64] The fwhm of the lasing emission peak is about 0.54 nm, as shown in Figure 4b. The quality factor Q is generally used to characterize the performance of the NW resonators, which is calculated by the following formula

https://doi.org/10.1021/acsanm.3c03173
ACS Appl. Nano Mater. 2023, 6, 17881−17889

$$Q = \lambda/\delta\lambda$$

where λ represents the wavelength of the stimulated emission mode and $\delta\lambda$ represents the fwhm of the emission peak. After calculation, the maximum Q factor of $CsPbBr_3$ NW is 995, which is higher than that of the lasing quality factor of the hybrid perovskite ($CH_3NH_3PbBr_3$, $Q \sim 500$),[65] indicating that these NWs have high-quality cavities, confirming the potential application of nanolasers.

Moreover, laser oscillation at different sizes is a unique way to realize mode tunable lasing. As shown in Figure 4d, when NWs are increased from 11 to 25 μm, the emission peak gradually red-shifts from 534.53 to 537.58 nm. This observation is due to the energy loss of photon oscillation in the resonant cavities, and the energy attenuation causes the red shift of emissions. We explored the reciprocal relationship between the laser mode spacing and wire length. The equation is shown as follows

$$\delta\lambda = \lambda^2/\{2L[n - \lambda(dn/d\lambda)]\}$$

where λ is the wavelength of emission peaks, L is the length of the wires, n is the refractive index (0.67), and $dn/d\lambda$ is the dispersion ($-6.89\ \mu m^{-1}$). The calculated mode spacing ($\delta\lambda$) and the reciprocal of the wire length ($1/L$) are shown in Figure 4e, and a linear relationship between the two factors can be observed clearly. We investigated the time-dependent stimulated emission intensity of $CsPbBr_3$ NWs placed in air under 355 nm pump pulse excitation at room temperature (Figure 4f), and the NWs continuously outputted stable laser light for more than 10 h, which is greatly improved compared to the hybrid perovskite nanolaser.[66] We stored the NWs under dry conditions for more than 3 months and no significant morphological changes.

Additionally, bandgap engineering of $CsPbBr_{3x}I_{3-3x}$ alloy perovskite NWs can be a good candidate for tunable nanoscale lasers. In Figure 5, obvious tunable lasing with a wavelength range from 538 to 699 nm is successfully realized at room temperature using these bandgap-tunable $CsPbBr_{3x}I_{3-3x}$ perovskite alloy NWs. The laser intensity of alloy NWs is slightly lower than the $CsPbBr_3$ NWs with an fwhm of about 0.65−0.96 nm, and the Q factors are 633−1075 respectively. Meanwhile, the lasing threshold of these alloy NWs is 35−45 μJ cm^{-2} (see Figure S8, Supporting Information), which is lower than those of hybrid perovskite (~60 μJ cm^{-2}) wires.[62] All of these results indicate that bandgap-tunable perovskite NWs are a good material platform for tunable nanolasers.

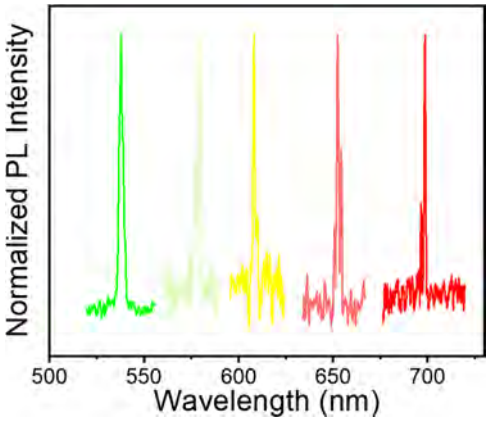

Figure 5. Wavelength-tunable emissions of bandgap-tunable $CsPbBr_{3x}I_{3-3x}$ alloy NWs at room temperature.

4. CONCLUSIONS

In summary, we developed a one-step source-moving CVD method to synthesize composition tunable $CsPbBr_{3x}I_{3-3x}$ alloy NWs. The bandgap of these alloy NWs can be continuously adjusted by controlling the growth temperature and reaction time during the anion exchange process. Structural characterizations and spectral investigations of these structures indicate that the obtained alloy wires are high-quality perovskite NWs with tunable PL emissions. Moreover, under a 355 nm pulse laser illumination, wavelength-tunable nanoscale lasers range from 538 to 699 nm with a Q_{max} factor of about 1075 at room temperature. These achievements represent significant advantages in the controllable growth of bandgap-tunable perovskite NWs, which may act as effective emission systems and have potential applications in high-performance integrated nanophotonic devices.

■ ASSOCIATED CONTENT

Supporting Information

The Supporting Information is available free of charge at https://pubs.acs.org/doi/10.1021/acsanm.3c03173.

Schematic diagram of the experiment setup for the synthesis of pure $CsPbBr_3$ and $CsPbI_3$ NWs; one-step source-moving CVD method for the perovskite alloy NWs; typical SEM image of as-grown $CsPbI_3$ alloy NWs; top-view enlarged SEM image of the wire; close-up SEM image of a single $CsPbI_3$ NWs; schematic diagram of the confocal optical system for optical measurement; and EDX profiles of $CsPbBr_{3x}I_{3-3x}$ perovskite alloy NWs with different compositions (PDF)

■ AUTHOR INFORMATION

Corresponding Authors

Pengfei Guo − *College of Electronic Information and Optical Engineering, Taiyuan University of Technology, Taiyuan 030024, China; Department of Materials Science and Engineering, City University of Hong Kong, Kowloon, Hong Kong 999077, China;* orcid.org/0000-0002-4785-0753; Email: guopengfei2010@126.com

Xia Shen − *College of Electronic Information and Optical Engineering, Taiyuan University of Technology, Taiyuan 030024, China*; Email: shenxia2019@126.com

Authors

Jie Fan − *College of Electronic Information and Optical Engineering, Taiyuan University of Technology, Taiyuan 030024, China*

Qihang Lv − *College of Electronic Information and Optical Engineering, Taiyuan University of Technology, Taiyuan 030024, China*

Xiaohang Song − *College of Electronic Information and Optical Engineering, Taiyuan University of Technology, Taiyuan 030024, China*

You Meng − *Department of Materials Science and Engineering, City University of Hong Kong, Kowloon, Hong Kong 999077, China*

Zitong Xu − *College of Electronic Information and Optical Engineering, Taiyuan University of Technology, Taiyuan 030024, China*

Jishen Wang − *College of Electronic Information and Optical Engineering, Taiyuan University of Technology, Taiyuan 030024, China*
Tingkai Xu − *College of Electronic Information and Optical Engineering, Taiyuan University of Technology, Taiyuan 030024, China*
Xuyang Li − *College of Electronic Information and Optical Engineering, Taiyuan University of Technology, Taiyuan 030024, China*
Liantuan Xiao − *College of Electronic Information and Optical Engineering, Taiyuan University of Technology, Taiyuan 030024, China;* orcid.org/0000-0003-2690-6460
Johnny C. Ho − *Department of Materials Science and Engineering, City University of Hong Kong, Kowloon, Hong Kong 999077, China;* orcid.org/0000-0003-3000-8794

Complete contact information is available at: https://pubs.acs.org/10.1021/acsanm.3c03173

Notes

The authors declare no competing financial interest.

■ ACKNOWLEDGMENTS

The authors thank Professor Huigao Duan (Hunan University) for helpful discussions. This work was financially supported by the start-up funding from Taiyuan University of Technology, the National Natural Science Foundation of China (no. 52373246), Shanxi Basic Research Program Project (no. 20210302123128), Graduate Education Innovation Program from Shanxi Provincial (no. 2022Y271), and a fellowship award from the Research Grants Council of the Hong Kong Special Administrative Region, China (CityURFS2021-1S04).

■ REFERENCES

(1) Fu, Y.; Zhu, H.; Chen, J.; Hautzinger, M. P.; Zhu, X. Y.; Jin, S. Metal halide perovskite nanostructures for optoelectronic applications and the study of physical properties. *Nat. Rev. Mater.* **2019**, *4*, 169−188.
(2) Pauzauskie, P. J.; Yang, P. Nanowire photonics. *Mater. Today* **2006**, *9*, 36−45.
(3) Zhang, Q.; Ha, S. T.; Liu, X.; Sum, T. C.; Xiong, Q. Room-temperature near-infrared high-Q perovskite whispering-gallery planar nanolasers. *Nano Lett.* **2014**, *14*, 5995−6001.
(4) Zhu, H.; Fu, Y.; Meng, F.; Wu, X.; Gong, Z.; Ding, Q.; Gustafsson, M. V.; Trinh, M. T.; Jin, S.; Zhu, X. Y. Lead halide perovskite nanowire lasers with low lasing thresholds and high quality factors. *Nat. Mater.* **2015**, *14*, 636−642.
(5) Guo, P.; Yang, Q.; Shen, X.; Lv, Q.; Hao, Y.; Xiao, L.; Ho, J. C.; Yu, K. M. Room-Temperature Broad-Wavelength-Tunable Single-Mode Lasing from Alloyed CdS(1-x)Se(x) Nanotripods. *ACS Nano* **2022**, *16*, 12767−12776.
(6) Zhou, H.; Yuan, S.; Wang, X.; Xu, T.; Wang, X.; Li, H.; Zheng, W.; Fan, P.; Li, Y.; Sun, L.; Pan, A. Vapor Growth and Tunable Lasing of Band Gap Engineered Cesium Lead Halide Perovskite Micro/Nanorods with Triangular Cross Section. *ACS Nano* **2017**, *11*, 1189−1195.
(7) Zhang, Q.; Su, R.; Liu, X.; Xing, J.; Sum, T. C.; Xiong, Q. High-Quality Whispering-Gallery-Mode Lasing from Cesium Lead Halide Perovskite Nanoplatelets. *Adv. Funct. Mater.* **2016**, *26*, 6238−6245.
(8) Li, H.; Li, J.; Bao, Y.; Li, J.; He, C.; Wang, H.; Zhang, Y.; Tang, H.; Xu, J.; Fang, Y.; Liang, S.; Yang, Y. A liquid phase anion-exchange approach to high-quality all-inorganic halide perovskite micro- and nanowires. *J. Mater. Sci.* **2021**, *56*, 16059−16067.
(9) Tang, X.; Zu, Z.; Shao, H.; Hu, W.; Zhou, M.; Deng, M.; Chen, W.; Zang, Z.; Zhu, T.; Xue, J. All-inorganic perovskite CsPb(Br/I)3 nanorods for optoelectronic application. *Nanoscale* **2016**, *8*, 15158−15161.
(10) Deng, W.; Huang, L.; Xu, X.; Zhang, X.; Jin, X.; Lee, S. T.; Jie, J. Ultrahigh-Responsivity Photodetectors from Perovskite Nanowire Arrays for Sequentially Tunable Spectral Measurement. *Nano Lett.* **2017**, *17*, 2482−2489.
(11) Tang, X.; Zhou, H.; Pan, X.; Liu, R.; Wu, D.; Wang, H. All-Inorganic Halide Perovskite Alloy Nanowire Network Photodetectors with High Performance. *ACS Appl. Mater. Interfaces* **2020**, *12*, 4843−4848.
(12) Zhang, Q.; Shang, Q.; Su, R.; Do, T. T. H.; Xiong, Q. Halide Perovskite Semiconductor Lasers: Materials, Cavity Design, and Low Threshold. *Nano Lett.* **2021**, *21*, 1903−1914.
(13) Guo, P.; Liu, D.; Shen, X.; Lv, Q.; Wu, Y.; Yang, Q.; Li, P.; Hao, Y.; Ho, J. C.; Yu, K. M. On-wire axial perovskite heterostructures for monolithic dual-wavelength laser. *Nano Energy* **2022**, *92*, No. 106778.
(14) Li, F.; Yang, Z.; Jiang, M.; Wang, C.; Xi, J.; Zhang, Y.; Pan, C.; Lu, J.; Wang, R. Wavelength tunable single-mode lasing from cesium lead halide perovskite microwires. *Appl. Phys. Lett.* **2021**, *118*, No. 071103.
(15) Zhao, C.; Zhang, D.; Qin, C. Perovskite Light-Emitting Diodes. *CCS Chem.* **2020**, *2*, 859−869.
(16) Lin, K.; Xing, J.; Quan, L. N.; de Arquer, F. P. G.; Gong, X.; Lu, J.; Xie, L.; Zhao, W.; Zhang, D.; Yan, C.; Li, W.; Liu, X.; Lu, Y.; Kirman, J.; Sargent, E. H.; Xiong, Q.; Wei, Z. Perovskite light-emitting diodes with external quantum efficiency exceeding 20%. *Nature* **2018**, *562*, 245−248.
(17) Xu, J.; Zhuang, X.; Guo, P.; Huang, W.; Hu, W.; Zhang, Q.; Wan, Q.; Zhu, X.; Yang, Z.; Tong, L.; Duan, X.; Pan, A. Asymmetric light propagation in composition-graded semiconductor nanowires. *Sci. Rep.* **2012**, *2*, No. 820.
(18) Xu, J.; Zhuang, X.; Guo, P.; Zhang, Q.; Huang, W.; Wan, Q.; Hu, W.; Wang, X.; Zhu, X.; Fan, C.; Yang, Z.; Tong, L.; Duan, X.; Pan, A. Wavelength-Converted/Selective Waveguiding Based on Composition-Graded Semiconductor Nanowires. *Nano Lett.* **2012**, *12*, 5003−5007.
(19) Liang, J.; Wang, C.; Wang, Y.; Xu, Z.; Lu, Z.; Ma, Y.; Zhu, H.; Hu, Y.; Xiao, C.; Yi, X.; Zhu, G.; Lv, H.; Ma, L.; Chen, T.; Tie, Z.; Jin, Z.; Liu, J. All-Inorganic Perovskite Solar Cells. *J. Am. Chem. Soc.* **2016**, *138*, 15829−15832.
(20) Mishra, S.; Ghosh, S.; Singh, T. Progress in Materials Development for Flexible Perovskite Solar Cells and Future Prospects. *ChemSusChem* **2021**, *14*, 512−538.
(21) Tong, Y.; Najar, A.; Wang, L.; Liu, L.; Du, M.; Yang, J.; Li, J.; Wang, K.; Liu, S. F. Wide-Bandgap Organic-Inorganic Lead Halide Perovskite Solar Cells. *Adv. Sci.* **2022**, *9*, No. 2105085.
(22) Docampo, P.; Ball, J. M.; Darwich, M.; Eperon, G. E.; Snaith, H. J. Efficient organometal trihalide perovskite planar-heterojunction solar cells on flexible polymer substrates. *Nat. Commun.* **2013**, *4*, No. 2761.
(23) Nie, W.; Tsai, H.; Asadpour, R.; Blancon, J. C.; Neukirch, A. J.; Gupta, G.; Crochet, J. J.; Chhowalla, M.; Tretiak, S.; Alam, M. A.; Wang, H.-L.; Mohite, A. D. High-efficiency solution-processed perovskite solar cells with millimeter-scale grains. *Science* **2015**, *347*, 522−525.
(24) Ning, C. Z.; Dou, L.; Yang, P. Bandgap engineering in semiconductor alloy nanomaterials with widely tunable compositions. *Nat. Rev. Mater.* **2017**, *2*, No. 17070.
(25) Lai, M.; Obliger, A.; Lu, D.; Kley, C. S.; Bischak, C. G.; Kong, Q.; Lei, T.; Dou, L.; Ginsberg, N. S.; Limmer, D. T.; Yang, P. Intrinsic anion diffusivity in lead halide perovskites is facilitated by a soft lattice. *Proc. Natl. Acad. Sci. U.S.A.* **2018**, *115*, 11929−11934.
(26) Huang, L.; Gao, Q.; Sun, L. D.; Dong, H.; Shi, S.; Cai, T.; Liao, Q.; Yan, C. H. Composition-Graded Cesium Lead Halide Perovskite Nanowires with Tunable Dual-Color Lasing Performance. *Adv. Mater.* **2018**, *30*, No. 1800596.
(27) Ha, S. T.; Su, R.; Xing, J.; Zhang, Q.; Xiong, Q. Metal halide perovskite nanomaterials: synthesis and applications. *Chem. Sci.* **2017**, *8*, 2522−2536.
(28) Nedelcu, G.; Protesescu, L.; Yakunin, S.; Bodnarchuk, M. I.; Grotevent, M. J.; Kovalenko, M. V. Fast Anion-Exchange in Highly Luminescent Nanocrystals of Cesium Lead Halide Perovskites ($CsPbX_3$, X = Cl, Br, I). *Nano Lett.* **2015**, *15*, 5635−5640.

(29) Pan, D.; Fu, Y.; Chen, J.; Czech, K. J.; Wright, J. C.; Jin, S. Visualization and Studies of Ion-Diffusion Kinetics in Cesium Lead Bromide Perovskite Nanowires. *Nano Lett.* **2018**, *18*, 1807−1813.
(30) Tian, W.; Leng, J.; Zhao, C.; Jin, S. Long-Distance Charge Carrier Funneling in Perovskite Nanowires Enabled by Built-in Halide Gradient. *J. Am. Chem. Soc.* **2017**, *139*, 579−582.
(31) Brenner, P.; Glöckler, T.; Rueda-Delgado, D.; Abzieher, T.; Jakoby, M.; Richards, B. S.; Paetzold, U. W.; Howard, I. A.; Lemmer, U. Triple cation mixed-halide perovskites for tunable lasers. *Opt. Mater. Express* **2017**, *7*, 4082−4094.
(32) Hu, Z.; Lin, Z.; Su, J.; Zhang, J.; Chang, J.; Hao, Y. A Review on Energy Band-Gap Engineering for Perovskite Photovoltaics. *Solar RRL* **2019**, *3*, No. 1900304.
(33) Cen, G.; Xia, Y.; Zhao, C.; Fu, Y.; An, Y.; Yuan, Y.; Shi, T.; Mai, W. Precise Phase Control of Large-Scale Inorganic Perovskites via Vapor-Phase Anion-Exchange Strategy. *Small* **2020**, *16*, No. 2005226.
(34) Jiang, H.; Cui, S.; Chen, Y.; Zhong, H. Ion exchange for halide perovskite: From nanocrystal to bulk materials. *Nano Select* **2021**, *2*, 2040−2060.
(35) Akkerman, Q. A.; D'Innocenzo, V.; Accornero, S.; Scarpellini, A.; Petrozza, A.; Prato, M.; Manna, L. Tuning the Optical Properties of Cesium Lead Halide Perovskite Nanocrystals by Anion Exchange Reactions. *J. Am. Chem. Soc.* **2015**, *137*, 10276−10281.
(36) Dey, A.; Ye, J.; De, A.; Debroye, E.; Ha, S. K.; Bladt, E.; Kshirsagar, A. S.; Wang, Z.; Yin, J.; Wang, Y.; Quan, L. N.; Yan, F.; Gao, M.; Li, X.; Shamsi, J.; Debnath, T.; Cao, M.; Scheel, M. A.; Kumar, S.; Steele, J. A.; Gerhard, M.; Chouhan, L.; Xu, K.; Wu, X. G.; Li, Y.; Zhang, Y.; Dutta, A.; Han, C.; Vincon, I.; Rogach, A. L.; Nag, A.; Samanta, A.; Korgel, B. A.; Shih, C. J.; Gamelin, D. R.; Son, D. H.; Zeng, H.; Zhong, H.; Sun, H.; Demir, H. V.; Scheblykin, I. G.; Mora-Sero, I.; Stolarczyk, J. K.; Zhang, J. Z.; Feldmann, J.; Hofkens, J.; Luther, J. M.; Perez-Prieto, J.; Li, L.; Manna, L.; Bodnarchuk, M. I.; Kovalenko, M. V.; Roeffaers, M. B. J.; Pradhan, N.; Mohammed, O. F.; Bakr, O. M.; Yang, P.; Muller-Buschbaum, P.; Kamat, P. V.; Bao, Q.; Zhang, Q.; Krahne, R.; Galian, R. E.; Stranks, S. D.; Bals, S.; Biju, V.; Tisdale, W. A.; Yan, Y.; Hoye, R. L. Z.; Polavarapu, L. State of the Art and Prospects for Halide Perovskite Nanocrystals. *ACS Nano* **2021**, *15*, 10775−10981.
(37) Cha, H.; Bae, S.; Jung, H.; Ko, M. J.; Jeon, H. Single-Mode Distributed Feedback Laser Operation in Solution-Processed Halide Perovskite Alloy System. *Adv. Opt. Mater.* **2017**, *5*, No. 1700545.
(38) Markina, D. I.; Anoshkin, S. S.; Masharin, M. A.; Khubezhov, S. A.; Tzibizov, I.; Dolgintsev, D.; Terterov, I. N.; Makarov, S. V.; Pushkarev, A. P. Perovskite Nanowire Laser for Hydrogen Chloride Gas Sensing. *ACS Nano* **2023**, *17*, 1570−1582.
(39) Zhang, G.; Song, P.; Shen, Z.; Qiao, B.; Song, D.; Cao, J.; Xu, Z.; Swelm, W.; Al-Ghamdi, A.; Zhao, S. $CsPbBr_{(3)}$@$CsPbBr_{(3-x)}Cl_{(x)}$ Perovskite Core-Shell Heterojunction Nanowires via a Postsynthetic Method with HCl Gas. *ACS Omega* **2020**, *5*, 11578−11584.
(40) Dou, L.; Lai, M.; Kley, C. S.; Yang, Y.; Bischak, C. G.; Zhang, D.; Eaton, S. W.; Ginsberg, N. S.; Yang, P. Spatially resolved multicolor CsPbX3 nanowire heterojunctions via anion exchange. *Proc. Natl. Acad. Sci. U.S.A.* **2017**, *114*, 7216−7221.
(41) Li, J.; Xu, J.; Bao, Y.; Li, J.; Wang, H.; He, C.; An, M.; Tang, H.; Sun, Z.; Fang, Y.; Liang, S.; Yang, Y. Anion-Exchange Driven Phase Transition in $CsPbI_3$ Nanowires for Fabricating Epitaxial Perovskite Heterojunctions. *Adv. Mater.* **2022**, *34*, No. 2109867.
(42) Wang, M.; Tian, W.; Cao, F.; Wang, M.; Li, L. Flexible and Self-Powered Lateral Photodetector Based on Inorganic Perovskite $CsPbI_3$−$CsPbBr_3$ Heterojunction Nanowire Array. *Adv. Funct. Mater.* **2020**, *30*, No. 1909771.
(43) Massasa, E. H.; Strassberg, R.; Vurgaft, A.; Kauffmann, Y.; Cohen, N.; Bekenstein, Y. Thin Layer Buckling in Perovskite $CsPbBr_3$ Nanobelts. *Nano Lett.* **2021**, *21*, 5564−5571.
(44) Tang, B.; Hu, Y.; Lu, J.; Dong, H.; Mou, N.; Gao, X.; Wang, H.; Jiang, X.; Zhang, L. Energy transfer and wavelength tunable lasing of single perovskite alloy nanowire. *Nano Energy* **2020**, *71*, No. 104641.
(45) Fu, Y.; Poddar, S.; Ren, B.; Xie, Y.; Zhang, Q.; Zhang, D.; Cao, B.; Tang, Y.; Ding, Y.; Qiu, X.; Shu, L.; Liao, J. F.; Kuang, D. B.; Fan, Z. Strongly Quantum-Confined Perovskite Nanowire Arrays for Color-Tunable Blue-Light-Emitting Diodes. *ACS Nano* **2022**, *16*, 8388−8398.
(46) Park, K.; Lee, J. W.; Kim, J. D.; Han, N. S.; Jang, D. M.; Jeong, S.; Park, J.; Song, J. K. Light-Matter Interactions in Cesium Lead Halide Perovskite Nanowire Lasers. *J. Phys. Chem. Lett.* **2016**, *7*, 3703−3710.
(47) Meng, Y.; Lan, C.; Li, F.; Yip, S.; Wei, R.; Kang, X.; Bu, X.; Dong, R.; Zhang, H.; Ho, J. C. Direct Vapor-Liquid-Solid Synthesis of All-Inorganic Perovskite Nanowires for High-Performance Electronics and Optoelectronics. *ACS Nano* **2019**, *13*, 6060−6070.
(48) Lim, S.; Ha, M.; Lee, Y.; Ko, H. Large-Area, Solution-Processed, Hierarchical $MAPbI_3$ Nanoribbon Arrays for Self-Powered Flexible Photodetectors. *Adv. Opt. Mater.* **2018**, *6*, No. 1800615.
(49) Zhu, B. S.; He, Z.; Yao, J. S.; Chen, C.; Wang, K. H.; Yao, H.-B.; Liu, J. W.; Yu, S. H. Potassium Ion Assisted Synthesis of Organic-Inorganic Hybrid Perovskite Nanobelts for Stable and Flexible Photodetectors. *Adv. Opt. Mater.* **2018**, *6*, No. 1701029.
(50) Deng, W.; Zhang, X.; Huang, L.; Xu, X.; Wang, L.; Wang, J.; Shang, Q.; Lee, S. T.; Jie, J. Aligned Single-Crystalline Perovskite Microwire Arrays for High-Performance Flexible Image Sensors with Long-Term Stability. *Adv. Mater.* **2016**, *28*, 2201−2208.
(51) Wang, Y.; Guan, X.; Li, D.; Cheng, H. C.; Duan, X.; Lin, Z.; Duan, X. Chemical vapor deposition growth of single-crystalline cesium lead halide microplatelets and heterostructures for optoelectronic applications. *Nano Res.* **2017**, *10*, 1223−1233.
(52) Ji, Z.; Liu, Y.; Zhao, C.; Wang, Z. L.; Mai, W. Perovskite Wide-Angle Field-Of-View Camera. *Adv. Mater.* **2022**, *34*, No. 2206957.
(53) He, C.; Liu, X. The rise of halide perovskite semiconductors. *Light: Sci. Appl.* **2023**, *12*, No. 15.
(54) Shamsi, J.; Urban, A. S.; Imran, M.; De Trizio, L.; Manna, L. Metal Halide Perovskite Nanocrystals: Synthesis, Post-Synthesis Modifications, and Their Optical Properties. *Chem. Rev.* **2019**, *119*, 3296−3348.
(55) Eaton, S. W.; Lai, M.; Gibson, N. A.; Wong, A. B.; Dou, L.; Ma, J.; Wang, L. W.; Leone, S. R.; Yang, P. Lasing in robust cesium lead halide perovskite nanowires. *Proc. Natl. Acad. Sci. U.S.A.* **2016**, *113*, 1993−1998.
(56) Schlaus, A. P.; Spencer, M. S.; Miyata, K.; Liu, F.; Wang, X.; Datta, I.; Lipson, M.; Pan, A.; Zhu, X. Y. How lasing happens in $CsPbBr_3$ perovskite nanowires. *Nat. Commun.* **2019**, *10*, No. 265.
(57) Wang, L.; Fu, L.; Yin, L. SnS Quantum Dot−$CsPbBr_3$ Perovskite Bulk Heterojunction for Enhanced Photoelectrical Conversion Efficiency. *Solar RRL* **2020**, *4*, No. 2000417.
(58) Wang, X.; Shoaib, M.; Wang, X.; Zhang, X.; He, M.; Luo, Z.; Zheng, W.; Li, H.; Yang, T.; Zhu, X.; Ma, L.; Pan, A. High-Quality In-Plane Aligned $CsPbX_3$ Perovskite Nanowire Lasers with Composition-Dependent Strong Exciton-Photon Coupling. *ACS Nano* **2018**, *12*, 6170−6178.
(59) Quan, L. N.; Kang, J.; Ning, C. Z.; Yang, P. Nanowires for Photonics. *Chem. Rev.* **2019**, *119*, 9153−9169.
(60) Zhang, Y.; Lu, D.; Gao, M.; Lai, M.; Lin, J.; Lei, T.; Lin, Z.; Quan, L. N.; Yang, P. Quantitative imaging of anion exchange kinetics in halide perovskites. *Proc. Natl. Acad. Sci. U.S.A.* **2019**, *116*, 12648−12653.
(61) Fu, Y.; Zhu, H.; Stoumpos, C. C.; Ding, Q.; Wang, J.; Kanatzidis, M. G.; Zhu, X.; Jin, S. Broad Wavelength Tunable Robust Lasing from Single-Crystal Nanowires of Cesium Lead Halide Perovskites ($CsPbX_3$, X = Cl, Br, I). *ACS Nano* **2016**, *10*, 7963−7972.
(62) Xing, J.; Liu, X. F.; Zhang, Q.; Ha, S. T.; Yuan, Y. W.; Shen, C.; Sum, T. C.; Xiong, Q. Vapor Phase Synthesis of Organometal Halide Perovskite Nanowires for Tunable Room-Temperature Nanolasers. *Nano Lett.* **2015**, *15*, 4571−4577.
(63) Lignos, I.; Stavrakis, S.; Nedelcu, G.; Protesescu, L.; deMello, A. J.; Kovalenko, M. V. Synthesis of Cesium Lead Halide Perovskite Nanocrystals in a Droplet-Based Microfluidic Platform: Fast Parametric Space Mapping. *Nano Lett.* **2016**, *16*, 1869−1877.
(64) Tian, X.; Wang, L.; Li, W.; Lin, Q.; Cao, Q. Whispering Gallery Mode Lasing from Perovskite Polygonal Microcavities via Femtosecond Laser Direct Writing. *ACS Appl. Mater. Interfaces* **2021**, *13*, 16952−16958.

https://doi.org/10.1021/acsanm.3c03173
ACS Appl. Nano Mater. 2023, 6, 17881−17889

(65) Liu, P.; He, X.; Ren, J.; Liao, Q.; Yao, J.; Fu, H. Organic–Inorganic Hybrid Perovskite Nanowire Laser Arrays. *ACS Nano* **2017**, *11*, 5766−5773.
(66) Fu, Y.; Zhu, H.; Schrader, A. W.; Liang, D.; Ding, Q.; Joshi, P.; Hwang, L.; Zhu, X. Y.; Jin, S. Nanowire Lasers of Formamidinium Lead Halide Perovskites and Their Stabilized Alloys with Improved Stability. *Nano Lett.* **2016**, *16*, 1000−1008.

https://doi.org/10.1021/acsanm.3c03173
ACS Appl. Nano Mater. 2023, 6, 17881−17889